



## Research article

# An online detection method for municipal sludge moisture content based on ultrasonic transmission technology



Yan Zhang<sup>a</sup>, Zhichao Zheng<sup>a</sup>, Fudong Gong<sup>b</sup>, Shu Cheng<sup>c</sup>, Hao Xu<sup>d</sup>, Zhongzhong Zhang<sup>a</sup>, Yawen Yao<sup>a</sup>, Binqi Rao<sup>a,\*</sup>

<sup>a</sup> School of Mechanical and Electrical Engineering, China Jiliang University, Hangzhou, 310018, China

<sup>b</sup> Zhejiang Qianjiang Water Conservancy & Supply Co., Ltd., Hangzhou, 311201, China

<sup>c</sup> University of Shanghai for Science and Technology, Shanghai, 200093, China

<sup>d</sup> Zhejiang Lanxi Hongshi Holding Group Co., Ltd., Lanxi, 321100, China

## ARTICLE INFO

### Keywords:

Municipal sludge  
Moisture content determination  
Ultrasonic transmission method  
Multiple mixed regression model

## ABSTRACT

Accurate, real-time moisture content (MC) detection for municipal sludge is critical for optimizing dewatering and reducing treatment costs, which is difficult to implement due to its extremely complex physical and chemical properties. This study develops a novel online detection method, integrating ultrasonic transmission with a multivariate mixed regression (MMR) model, for non-destructive, high-precision online MC detection. Device geometry was optimized via COMSOL simulation, selecting a 40 kHz emission frequency and an 8 cm container distance, which together balance cavitation effects, energy dissipation, and cost-effectiveness. An experimental device incorporating adaptive density correction and temperature compensation was built, achieving stable measurements with a rapid response (<15 s). The dedicated MMR model was specifically designed for this system's characteristics and rigorously evaluated against multivariate linear regression (MLR) and back-propagation neural network (BPNN) models using identical data. Results demonstrate the MMR model's superiority: achieving an  $R^2$  of 0.978, MAE of 1.901, and RMSE of 2.233. Compared to the MLR and BPNN models, the MMR model increases  $R^2$  by 12.08 % and 10.37 %, respectively, while reducing MAE by 54.71 % and 52.91 %, and RMSE by 58.44 % and 56.16 %. The model was further validated using 30 sludge samples from different treatment plants, confirming its robustness and generalizability. This research provides a rapid, accurate, and stable solution for online MC detection, holding significant potential for real-time dewatering process optimization.

## 1. Introduction

Municipal sludge, a primary byproduct of wastewater treatment processes, has emerged as a critical challenge in global water environmental governance owing to the technical and logistical complexities inherent in its sustainable treatment and disposal. Within China's municipal infrastructure, the annual production of dewatered sludge from wastewater treatment plants (WWTPs) has exceeded 75 million metric tons, with sludge-related disposal costs constituting 30–50 % of total WWTP operational expenditures (Nguyen et al., 2021). In sludge management systems, the MC is a crucial technical parameter. Accurate measurement and real-time control of this parameter not only directly determine the energy consumption and material consumption during the dewatering process and the cost of selecting the disposal method, but

also determine whether the final disposal can meet the environmental protection standards (Yuan and Zhu, 2024). Moreover, due to the lack of reliable in-situ detection technology at present, problems such as excessive chemical agent addition and energy waste of dewatering equipment are widespread in industrial sites (Li et al., 2024). This makes real-time and precise monitoring and control of MC a key factor in optimizing the efficiency of sludge treatment and ensuring the economic feasibility of disposal operations. Conventional municipal WWTP operations predominantly employ mechanical dewatering coupled with chemical conditioning to reduce raw sludge moisture from 95 to 99 % to compliance thresholds of  $\leq 60$  % for landfilling or  $\leq 30$  % for thermal treatment (Liu et al., 2024). Nevertheless, real-time accurate detection of sludge MC in coupled mechanical-chemical dewatering process streams persists as a critical technical barrier, primarily due to dynamic

\* Corresponding author.

E-mail addresses: [20A0104183@cjlu.edu.cn](mailto:20A0104183@cjlu.edu.cn) (Y. Zhang), [raobinqi@cjlu.edu.cn](mailto:raobinqi@cjlu.edu.cn) (B. Rao).

physicochemical interactions and heterogeneous material characteristics. This technical challenge originates in the inherent physicochemical complexity of municipal sludge systems, characterized by dynamic colloidal transformations and persistent multiphase heterogeneity. It comprises not only a diverse array of solid constituents—including organic matter, inorganic particles, microorganisms, and their metabolic byproducts—but also harbors internal moisture existing in multiple states, such as free, interstitial, surface, and bound water (Mazurek et al., 2023). The intrinsic physicochemical complexity and structural heterogeneity of sludge matrices fundamentally undermine the measurement reliability of conventional rapid analytical methods. Consequently, the establishment of robust analytical frameworks accommodating the physicochemical complexity of municipal sludge matrices while providing real-time *in situ* quantification of MC has become a critical requirement for technological advancement in wastewater treatment infrastructure.

Although oven drying (oven drying at  $105 \pm 2^\circ\text{C}$ ) remains the industry standard for measuring MC, its prolonged processing time ( $>24$  h) and reliance on destructive sampling fundamentally limit its applicability in modern sludge management systems (Lin et al., 2020). Consequently, it is unsuitable for real-time process control in wastewater treatment plants, where immediate feedback on MC is required (Zhang et al., 2025). As a result, chemical overdosing is common, and dewatering equipment often operates for extended periods under sub-optimal conditions. Real-time detection technologies such as microwave dielectric analysis and near-infrared spectroscopy have attracted growing interest, but their implementation in municipal sludge systems remains constrained by significant industrial limitations. Among various techniques, the microwave method for detecting sludge MC primarily depends on the dielectric properties of the sludge (An et al., 2023; Li et al., 2021, 2022). However, these dielectric properties exhibit high sensitivity to temperature variations (Tang et al., 2019). In the thermally dynamic environments of industrial sites, this sensitivity often leads to deviations in MC detection, prompting operators to increase chemical safety margins to mitigate the risk of dewatering failure. However, near-infrared spectroscopy still faces substantial challenges in practical industrial applications. It imposes stringent requirements on detection conditions and sample uniformity. The intense optical scattering caused by sludge particles not only reduces model sensitivity but also necessitates frequent maintenance, incurs high calibration costs, and makes it difficult to reliably analyze the non-uniform sludge samples commonly encountered in industrial settings (Hong et al., 2021; Jia et al., 2020; Liu et al., 2022). Furthermore, most existing models for sludge moisture content estimation primarily focus on constructing empirical or data-driven relationships, with relatively limited attention given to the underlying mechanisms of key physical variables and their associated compensation strategies. Thus, the inherent limitations of existing methods under real-world industrial conditions have motivated researchers to pursue the development of novel non-destructive testing approaches for municipal sludge that address the challenges of accuracy and applicability in complex operational environments.

Ultrasonic technology offers clear advantages for MC detection. Technically, its high sensitivity to critical material parameters such as bulk density, internal porosity, and microstructural variations enables rapid and accurate measurements, even in heterogeneous or challenging environments (Wang et al., 2022). Economically, the fully non-contact configuration prevents probe wear and sample contamination, thereby reducing routine maintenance, operational downtime, and sensor replacement costs. Research has demonstrated a significant correlation between the ultrasonic wave propagation speed and the particle characteristics of sludge. Furthermore, ultrasonic treatment improves sludge settling characteristics and dewatering performance, thereby enhancing the release efficiency of organic matter during treatment. These findings provide a foundation for the development of reliable industrial online detection and enhanced sludge treatment technologies (Xu et al., 2019). Meanwhile, the acoustic attenuation coefficient can effectively

characterize the aggregation behavior of particles in high-viscosity media, thereby providing powerful data for the microscopic characteristics that cannot be obtained by traditional methods (Jameel et al., 2022). Studies on compressed grain samples have shown that ultrasonic wave propagation speed is inversely proportional to MC. This relationship also holds for other hygroscopic materials, and under similar experimental conditions, ultrasonic measurements typically yield lower errors than traditional methods. These findings offer a useful reference for applications in areas such as municipal sludge treatment (Shao and Chu, 2021). Research on the correlation between acoustic parameters and MC demonstrated that artificial intelligence (AI)-driven algorithms significantly enhance detection accuracy in MC prediction (Yuan et al., 2021). Notably, the non-contact ultrasonic system has demonstrated industrial feasibility for detection soil MC. This system enables high-precision, non-invasive detection by measuring leakage Rayleigh waves, thereby avoiding the structural disturbances caused by conventional sensors (Woo et al., 2022). Based on these technical characteristics, the ultrasonic method effectively addresses the limitations of conventional industrial detection techniques for measuring material MC. Its non-contact design significantly reduces maintenance costs and minimizes the risk of sensor contamination. Moreover, its suitability for complex media and high measurement accuracy provides a solid foundation for precise process control. These advantages translate into economic benefits by enabling coordinated optimization of water usage and dewatering energy consumption, thereby reducing the operational costs of wastewater treatment plants.

Ultrasonic techniques for determining MC can be fundamentally categorized into two main approaches based on the signal propagation mode: reflection-based methods and transmission-based methods. The reflection method estimates MC by analyzing ultrasonic signals reflected from the surface or internal interfaces of the medium. However, its accuracy is highly sensitive to surface roughness and acoustic coupling quality, making it less effective for deep or heterogeneous media (Elvira et al., 2016; Weser et al., 2014; Zuljan, 2022). In contrast, the transmission method determines MC by measuring changes in the ultrasonic signal after it passes through the medium. Although this approach requires transducer placement on opposite sides of the sample, it inherently captures the bulk properties of the medium, making it particularly well-suited for analyzing non-uniform and highly attenuating materials, such as sludge (Okazaki et al., 2021; Wen et al., 2024; Zhang et al., 2022). By directly measuring the propagation velocity and attenuation of ultrasound within the sludge, the transmission method provides an estimate of the sample's average MC, thereby minimizing errors caused by localized heterogeneity that can affect reflection-based measurements. However, while ultrasonic transmission systems have been effectively applied to materials such as soil, grains, and porous solids, their direct application to municipal sludge remains both challenging and insufficiently studied. This is primarily due to the higher acoustic attenuation of sludge, irregular wave scattering, and the complex coupling between MC and internal structural characteristics. In addition, ultrasonic waves can induce nonlinear effects such as cavitation, structural deformation, and localized temperature increases in porous hygroscopic media. These effects complicate signal interpretation, especially in materials that undergo shrinkage and density fluctuations (El Jery et al., 2023). Unlike relatively homogeneous materials, sludge is a highly heterogeneous, multiphase, and non-Newtonian matrix. Dynamic processes such as floc collapse and pore structure evolution during ultrasonic treatment further interfere with wave propagation. For instance, ultrasound-induced disintegration of flocs may weaken the correlation between wave velocity and MC (Ruiz-Hernando et al., 2022). A predictive model for sludge moisture content must emphasize critical physical parameters to achieve superior accuracy and distinguish itself from conventional empirical or purely data-driven methods (Fan et al., 2023; Yoo et al., 2022). Therefore, although ultrasonic techniques are fundamentally applicable to sludge moisture detection, their effective implementation requires specifically designed experimental setups and

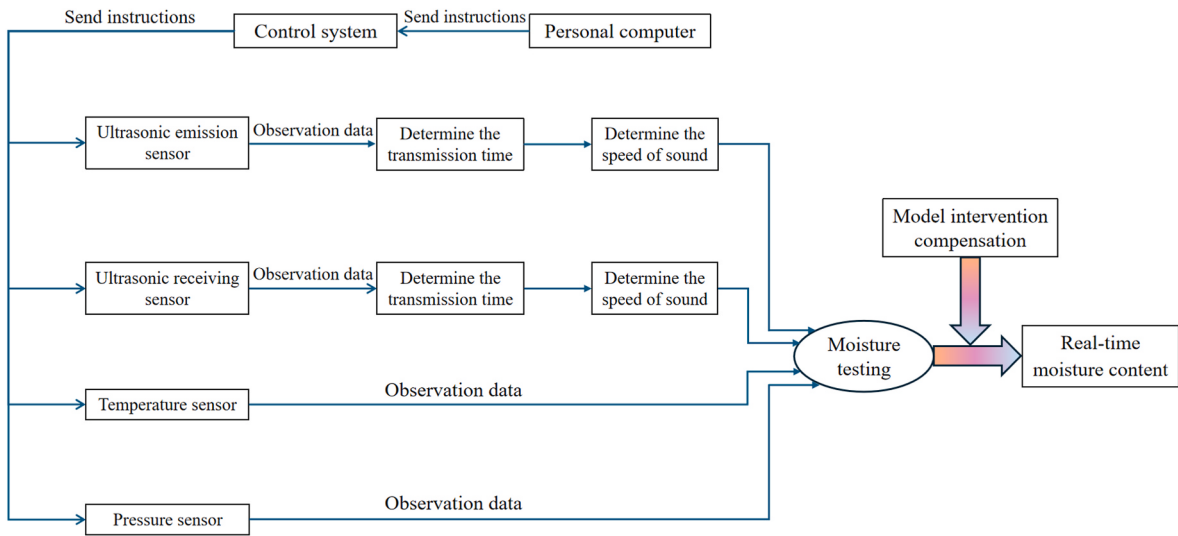


**Fig. 1.** Test procedure diagram of the device.

modeling strategies that can account for the nonlinear responses, temperature variation, and density changes associated with sludge, rather than directly applying systems originally developed for soil or grain.

In a word, although a variety of real-time detection techniques have been explored, each faces critical limitations under practical conditions. Oven drying is time-consuming and destructive, microwave dielectric methods are highly sensitive to ambient temperature, and near-infrared spectroscopy struggles with strong optical scattering and high calibration cost. Due to their respective limitations, these methods struggle to maintain stable performance in municipal sludge moisture content detection. Although ultrasonic transmission techniques have been successfully applied to materials such as soils and grains, their direct application to municipal sludge remains limited due to the material's pronounced acoustic attenuation, complex internal microstructure, and sensitivity to nonlinear effects such as density fluctuations and floc disintegration. To overcome these challenges, this study developed a robust, real-time ultrasonic transmission-based device specifically tailored for municipal sludge. The system adopts simulation-based optimization of sensor configuration and structural geometry, integrates adaptive bulk density correction and temperature compensation modules to enhance measurement stability, and introduces a novel piecewise modeling strategy, through which the MMR model enables accurate prediction of sludge MC under varying operational conditions. The detailed measurement workflow is illustrated in Fig. 1. This integrated framework is expected to significantly improve the accuracy, reliability, and industrial applicability of ultrasonic moisture detection in municipal sludge treatment.

## 2. Methodology

### 2.1. Principle analysis

Diverging from methodologies used for determining MC in other materials, sludge is a uniquely heterogeneous, particulate, and porous medium, primarily consisting of an admixture of dry solids, water, and air. When utilizing the ultrasonic transmission technique to quantify sludge MC, the acoustic waves emitted by the excitation transducer undergo attenuation as they propagate through this complex matrix.

This observed energy loss is primarily attributed to scattering phenomena induced by solid particles and viscous dissipation effects within the medium (Fan et al., 2023). Moreover, the propagation characteristics of ultrasound are significantly influenced by both the overall MC and its spatial distribution within the sludge.

Specifically, as the MC within the sludge increases, corresponding

changes occur in both the propagation velocity and attenuation characteristics of the ultrasonic waves. Consequently, analyzing these ultrasonic transmission properties allows for the assessment of sludge MC. To facilitate the quantification of these observed changes, we initially assume an idealized condition in which a unit volume of sludge contains  $N$  discrete scattering particles. Following this premise, the scattering attenuation coefficient, denoted  $a_s$ , is then computed using Eq. (1) (Waszcuk et al., 2023).

$$a_s = \frac{2}{9} N m^4 \pi r^6 \quad (1)$$

Where  $N$  is the particle number density (i.e., the number of particles per unit volume) ( $\text{m}^{-3}$ );  $m$  is the ultrasonic scattering wavenumber ( $\text{m}^{-1}$ ); and  $r$  is the radius of the scattering particles (m).

Building upon this foundation, the expression for the ultrasonic viscous attenuation coefficient was then derived using the model developed by S. van et al. (van den Wildenberg et al., 2020). This model represents an advancement based on the foundational work originally established by Urick, culminating in Eq. (2).

$$a_v = \emptyset \left[ \frac{1}{6} k^4 a^3 + k(\sigma - 1)^2 \frac{s}{s^2 + (\sigma + \tau)^2} \right] \quad (2)$$

Where  $\emptyset$  is the solid volume fraction;  $k$  is the wavenumber ( $\text{m}^{-1}$ );  $a$  is the particle radius (m);  $\sigma$  is the particle-to-fluid density ratio;  $\tau$  is the approximation of particle-fluid dynamic interactions; and  $s$  is a particle-characteristic parameter.

By consolidating the theoretical treatments of scattering attenuation ( $a_s$ ) and viscous attenuation ( $a_v$ ) previously outlined, the overall attenuation coefficient, denoted as  $a_t$ , is determined as their direct sum ( $a_t = a_s + a_v$ ). To achieve a more precise characterization of ultrasonic attenuation in the sludge medium, this study introduces Eq. (3). This formulation, derived under the self-consistent assumption, explicitly models these attenuation characteristics (Kamalinia and Tie, 2023).

$$a_t = -\frac{1}{D} \ln \left( \frac{U}{U_0} \right) \quad (3)$$

Where  $D$  represents the container distance of the ultrasonic wave within the medium (m);  $U_0$  denotes the incident ultrasonic amplitude (i.e., the amplitude before entering the medium); and  $U$  signifies the transmitted ultrasonic amplitude after container distance  $D$  through the medium.

Specifically, as the  $D$  increases, the inherent attenuation effects within the medium cause an exponential decay in the ultrasonic

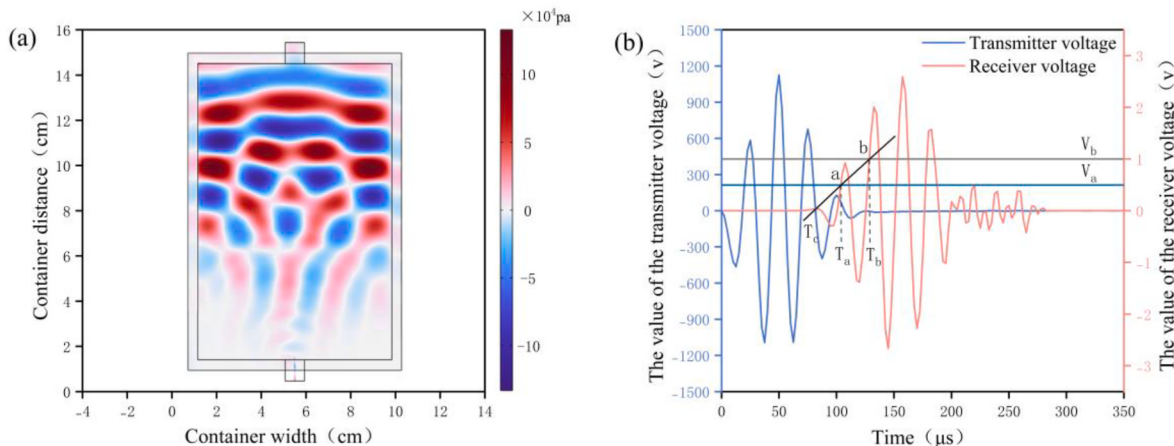


**Fig. 2.** (a) Spatial distribution map of acoustic pressure during ultrasonic propagation; (b) Temporal waveforms of the transmitted and received ultrasonic signals.

amplitude. Consequently, by systematically recording the ratio of  $U/U_0$  across varying container distances and applying the formulation presented in Equations (2) and (3), the specific value of the attenuation coefficient  $a_t$  can be rigorously determined. Furthermore, this acoustic attenuation coefficient exhibits significant frequency dependence, primarily manifested through the impact of frequency on scattering interactions during signal propagation. Ultrasonic waves with higher frequencies, characterized by shorter wavelengths, are considerably more susceptible to scattering by solid particulates suspended in the sludge. This heightened scattering leads to an increased signal attenuation rate, which adversely impacts measurement accuracy, an effect particularly pronounced at elevated MC levels (Brouwers et al., 2022). Conversely, lower-frequency ultrasonic waves have longer wavelengths, which afford them superior penetration capabilities and result in diminished scattering effects. This results in a lower acoustic attenuation coefficient and enhanced signal integrity. This inherent characteristic allows low-frequency ultrasound to maintain a superior signal-to-noise ratio (SNR) within the complex sludge matrix, thereby improving the precision of MC quantification (Qi et al., 2024). Therefore, a careful selection of the operating frequency, based on a thorough evaluation and trade-off analysis of frequency-dependent attenuation performance, is essential for optimizing the ultrasonic detection technique to achieve both effective and precise measurement of sludge MC.

## 2.2. Simulation results and analysis

Drawing on the principles outlined in Section 2.1, the careful selection of two key parameters within the ultrasonic detection system—specifically, the emission frequency and the container distance—is essential for achieving accurate measurements. Although the ultrasonic transmission phenomenon theoretically requires a three-dimensional model, this study utilizes a two-dimensional framework using COMSOL Multiphysics for simulation analysis. This simplification is justified because acoustic wave propagation within the detection container is primarily governed by its length, and a 2D representation provides an intuitive visualization of the ultrasonic wave's transit through the sludge medium. To rigorously mitigate the influence of boundary reflections on the simulation results, a Perfectly Matched Layer (PML) was incorporated around the transducer and the sludge structural domain. Through comprehensive simulation analyses evaluating acoustic propagation characteristics and the signal intensities that were received across various combinations of frequency and container distance, the optimal operational parameters were identified. The resultant simulation data effectively elucidates the dynamics of propagation and attenuation under varying parameter sets, thereby providing a robust theoretical foundation for the design of the practical system.

**Fig. 2(a)** presents a spatial distribution map that illustrates the simulated variations in acoustic pressure as the ultrasonic wave traverses the sludge interior. The accompanying color bar quantifies the intensity fluctuations of the acoustic pressure during its propagation within the detection apparatus. Variations in signal intensity are represented along both the positive and negative deviation axes. A red color gradient signifies the signal's behavior associated with positive pressure deviations. As the red hue intensifies, the pressure magnitude in the positive range increases, indicating enhanced signal strength during this phase. Conversely, a blue gradient depicts the signal's state associated with negative pressure deviations. A deeper blue coloration corresponds to increasingly negative pressure values, thereby representing augmented signal strength in the opposing phase. Collectively, the red-blue chromatic gradient visually encapsulates the dynamic changes experienced by the ultrasonic signal during its propagation through the sludge. Owing to the implementation of the PML, the intensity of the acoustic wave is effectively attenuated at the boundaries, thereby preventing spurious leakage into the external environment.

To further substantiate the viability of the simulation approach, this study primarily focuses on analyzing the propagation characteristics of ultrasound within the sludge by examining the source signal, as well as the transmitted and received signal waveforms. The source signal, representing the initial ultrasonic wave emitted by the transducer, was defined as a Gaussian-modulated sinusoidal pulse characterized by specific parameters to generate the transmitted waveform. Concurrently, a global probe was implemented to capture the received acoustic signal and convert it into the corresponding voltage values. The simulation duration was specified as 350 μs, employing a time step of 0.01 μs. The receiving transducer vibrates upon receiving the acoustic signal, subsequently converting this mechanical motion into an electrical signal. This observed behavior confirms that the simulated ultrasonic emission and reception processes function as anticipated, thereby theoretically validating the model's ability to accurately simulate ultrasonic transmission through the sludge medium. The temporal waveforms of the transmitted and received signals are illustrated in **Fig. 2(b)**. As shown therein, the transmitter initially generates a high-amplitude oscillatory signal. In contrast, the signal registered at the receiver exhibits a discernible time lag and significantly diminished amplitude, indicative of the attenuation and phase shift experienced by the wave during its propagation through the medium. Over time, the intensity of the received signal gradually attenuates and eventually stabilizes.

Recalling the preceding discussion regarding the acoustic pressure distribution map presented in **Fig. 2(a)**—which highlighted the formation of alternating zones of positive (red) and negative (blue) pressure within the propagation medium—this phenomenon can be further explained. By correlating this spatial pressure pattern with the

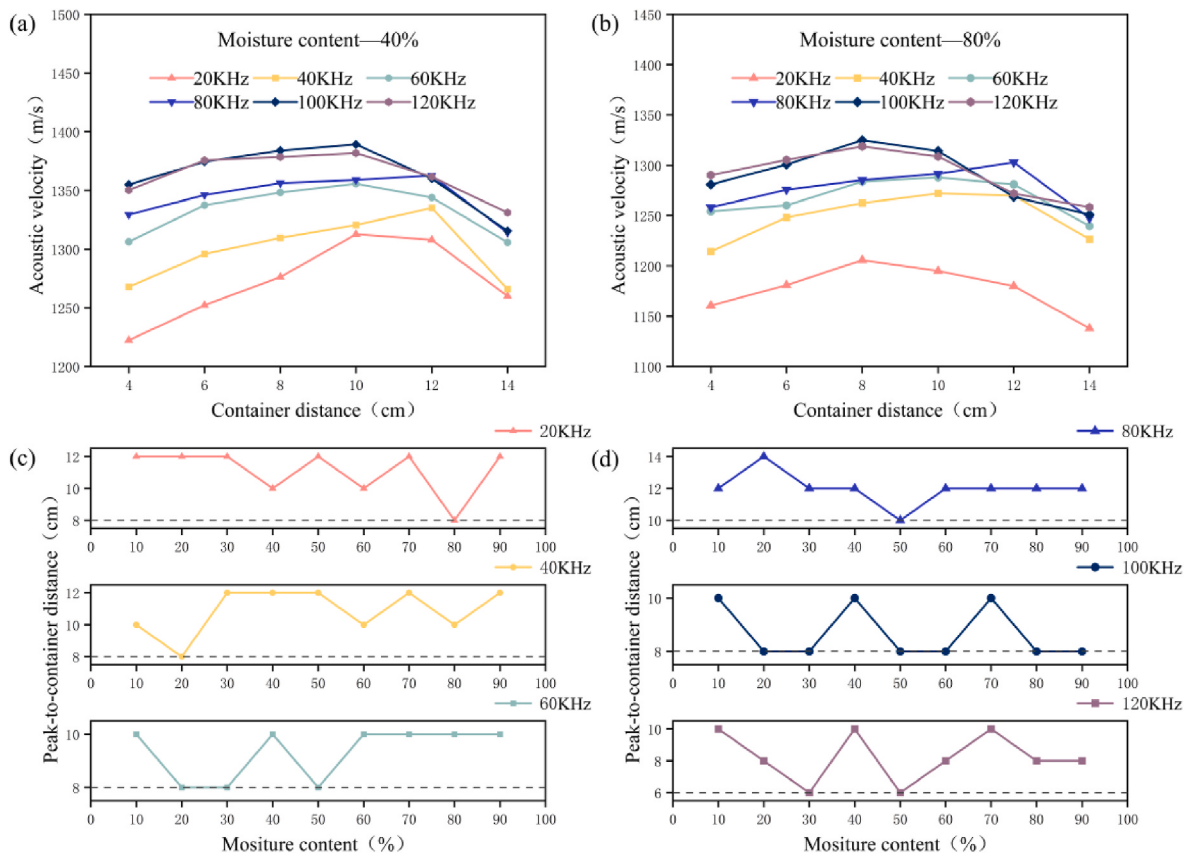


**Fig. 3.** (a) Acoustic velocity as a function of container distance for a MC of 40 %; (b) Acoustic velocity as a function of container distance for a MC of 80 %; (c-d) Container distance corresponding to the peak acoustic velocity plotted against MC for various emission frequencies.

sinusoidal voltage oscillation driving the transmitter (evident in the transmitted waveform shown in Fig. 2(b), the underlying mechanism becomes clear. Specifically, the sinusoidal alternation of the driving voltage generates a corresponding alternating acoustic pressure field within the medium, directly resulting in the sequential appearance of the positive and negative pressure regions observed in the simulation.

To facilitate accurate MC estimation, the calculation procedure involves three primary stages: (1) extraction of echo signal features using a dual-threshold method to determine the ultrasonic time-of-flight (TOF); (2) derivation of the acoustic velocity based on TOF and container distance; and (3) integration of acoustic parameters with empirical sludge properties through multivariate modeling. The associated equations and theoretical considerations for each stage are elaborated below. This study proposes a waveform feature resolution methodology based on a dual-threshold criterion, as shown in Fig. 2(b). This approach involves establishing distinct high ( $V_a$ ) and low ( $V_b$ ) voltage thresholds to capture two critical temporal points from the received echo signal:  $T_b$ , the trigger instant when the signal initially surpasses the high threshold  $V_a$ , and  $T_a$ , the time point marking the release from the low threshold  $V_b$  (typically occurring after the main pulse has passed). By integrating these temporal markers with the waveform characteristics of the ultrasonic signal's rising edge and utilizing Eq. (4), the actual arrival time ( $T_c$ ) of the ultrasonic echo can be precisely determined (Gover and Kopiński, 2022). Eq. (4) is based on linear interpolation between two voltage thresholds and captures the moment when the main pulse energy center arrives at the receiver. This method increases robustness against noise and waveform distortion, which are common in sludge environments. A comparative analysis of the transmitted and received signal waveforms, visualized on a common temporal axis, intuitively reveals the time delay and amplitude attenuation inherent in the signal's propagation through the sludge. This analysis facilitates the accurate calculation of the

ultrasonic time-of-flight (TOF) within the sludge medium, thereby providing a crucial empirical basis for optimizing the selection of appropriate operational parameters, namely the emission frequency and container distance within the container.

$$T_c = \frac{V_b T_a - V_a T_b}{V_b - V_a} \quad (4)$$

Where  $V_a$  represents the dynamic first threshold voltage (v);  $V_b$  denotes the dynamic second threshold voltage (v);  $T_a$  signifies the time instant corresponding to the release from the second threshold (s);  $T_b$  indicates the time instant when the signal initially surpasses the first threshold (s); and  $T_c$  constitutes the calculated actual arrival time of the echo (s).

During the process of determining the MC of sludge, fluctuations in MC inevitably induce changes in both the density and structural characteristics of the sludge. Such physicochemical alterations are directly and clearly reflected in the accompanying variations of the ultrasonic propagation velocity through the medium. Consequently, this study utilizes acoustic velocity as the primary parameter for characterizing these moisture-dependent changes. The governing equation for the velocity of ultrasound is given by Eq. (5):

$$v = \frac{l}{t} \quad (5)$$

Where  $l$  denotes the container distance traversed by the ultrasonic wave (cm);  $t$  signifies the corresponding acoustic TOF (ns).

Taking the derivative with respect to  $t$  yields the following Eq. (6):

$$dt = -\frac{v^2}{l} dv \quad (6)$$

Eq. (6) is used to determine how small a change in TOF must be detectable to reliably resolve changes in acoustic velocity. This provides

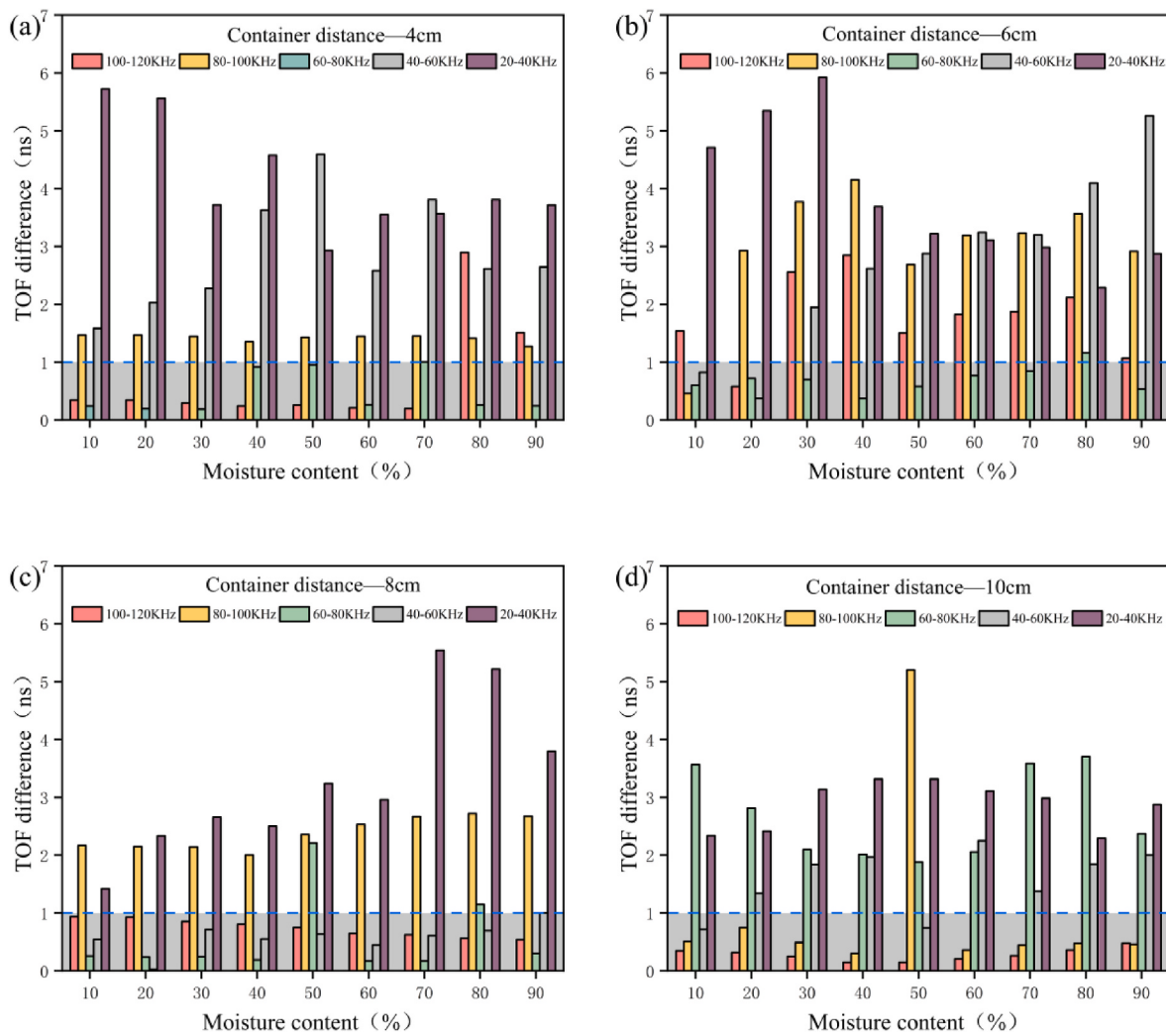


**Fig. 4.** Absolute differential TOF analysis for different container distances: (a) 4 cm, (b) 6 cm, (c) 8 cm, (d) 10 cm.

a quantitative basis for specifying the temporal resolution required by the data acquisition system. Applying Eq. (6) and assuming an acoustic velocity of 1800 m/s while considering container distances of 0.01 m and 0.02 m, the analysis reveals that the required precision for acoustic TOF measurement lies within the range of 0.617 ns–1.234 ns. Therefore, for this study, an acceptable error tolerance for TOF determination is established at approximately 1 ns.

The governing equation for determining the container distance is given by Eq. (7):

$$d = -\frac{\ln(S)}{a} \quad (7)$$

Where  $S$  denotes the sensitivity of the ultrasonic transducer;  $a$  signifies the attenuation coefficient characteristic of the sludge medium ( $\text{m}^{-1}$ ).

Acknowledging the significant impact of ultrasonic frequency on both dewatering efficiency and acoustic attenuation characteristics in sludge processing, this investigation focuses on simulations conducted across an emission frequency spectrum ranging from 20 kHz to 120 kHz. Nevertheless, before conducting the specific simulation analyses of sludge MC, it is essential to establish a suitable range for the container distance within the container. Eq. (7) links ultrasonic signal sensitivity to sludge attenuation, offering a theoretical limit for the container geometry under given sludge conditions. Based on Eq. (7), by assigning a value of  $e^{-3}$  to the sensitivity of the ultrasonic transducer and considering the sludge attenuation coefficient to range from a minimum of 10

to a maximum of 150, the theoretically permissible container distance was calculated to extend from 2 cm to 30 cm. However, considering the practical constraints that excessively long container distances would require substantial sludge sample volumes for experimental validation, the scope of the simulation model in this study was pragmatically limited to a container distance ranging from 4 cm to 14 cm. This defined range provides a well-circumscribed basis for the subsequent simulations, enhancing the robustness and applicability of the generated results.

This study begins by examining the interrelationship among emission frequency, container distance, acoustic velocity, and MC. To determine the optimal pairing of emission frequency and corresponding container distance, simulations were systematically conducted across a frequency spectrum ranging from 20 kHz to 120 kHz (in increments of 20 kHz), while also varying the container distance from 4 cm to 14 cm at 2 cm intervals. Given that the trend of acoustic velocity variation with increasing container distance remains qualitatively consistent across different MC for a fixed emission frequency, this paper presents the relational plots for MC of 40 % and 80 % only, as shown in Fig. 3(a–b). Inspection of Fig. 3(a–b) reveals that, under constant emission frequency conditions, the acoustic velocity exhibits a characteristic pattern of initially increasing and then subsequently decreasing as the container distance is extended. This phenomenon results from a dynamic equilibrium between acoustic attenuation and changes in the medium's structure. During the initial phase of wave propagation, the cavitation

effect induced by ultrasound disrupts the sludge floc structures, releasing bound water and promoting a more homogeneous medium. This homogenization consequently mitigates scattering losses, resulting in a temporary increase in acoustic velocity (Qi et al., 2024). However, as the wave travels greater distances, effects such as viscous absorption, thermal conduction, and scattering by sludge particulates become significantly more pronounced. This cumulative effect intensifies overall attenuation, leading to a gradual decline in acoustic velocity (Pilli et al., 2011). Throughout this process, the initial velocity-enhancing effect of medium homogenization is eventually surpassed by the dominant influence of energy dissipation mechanisms at greater distances, ultimately leading to the observed peak and turnaround characteristics of the velocity profile (Lounisnard, 2012). The ascending segment of the velocity curve is particularly significant because the homogenization effect is pronounced while energy losses remain relatively low during this phase. This regime is characterized by a potentially higher signal-to-noise ratio and enhanced stability, allowing for a clearer delineation of the intrinsic correlation between sludge structural changes and acoustic velocity (Zhu et al., 2018). Consequently, the container distances corresponding to this ascending velocity regime are selected as the optimal operational range in this study.

To enable a comprehensive evaluation of the optimal pairings between emission frequency and the container distance corresponding to the peak acoustic velocity at varying MC, this study presents plots (Fig. 3 (c-d)) that illustrate the relationship between MC and the container distance at which this velocity peak occurs. These analyses were conducted for five distinct emission frequencies ranging from 20 kHz to 120 kHz, in 20 kHz increments. As specifically illustrated in Fig. 2(c), for the 20 kHz emission frequency, the peak acoustic velocity is consistently achieved at or beyond a container distance of 8 cm across the entire evaluated MC range (10 %–90 %). This finding consequently defines the optimal operational range for 20 kHz, corresponding to the previously identified ascending velocity segment, as extending from 4 cm to 8 cm. Synthesizing these findings across the full frequency spectrum (20 kHz–120 kHz), the following operational strategies, encompassing preferred parameter combinations, were delineated: first, utilizing a container distance confined to the 4 cm–6 cm range, which is potentially applicable across all tested frequencies as a conservative baseline; Second, employing a broader range of 4 cm–8 cm, which has been specifically validated as optimal for the frequencies of 20, 40, 60, and 100 kHz; and third, extending the operational window to 4 cm–10 cm, which is identified as advantageous exclusively for the 80 kHz frequency. These selections represent the empirically derived optimal configurations based on the results of the simulations.

To refine the selection of the optimal emission frequency and the corresponding container distance combination, this study conducted a comparative analysis of the variations in propagation time between adjacent emission frequency bands at different fixed container distances. This differential approach not only elucidates the trend of the frequency's influence on TOF but also facilitates the selection of the most appropriate frequency band, guided by the established measurement precision requirements. Specifically, simulations were performed for container distances of 4 cm, 6 cm, 8 cm, and 10 cm, examining incremental frequency bands (e.g., 20–40 kHz, 40–60 kHz, and up to 100–120 kHz) across an MC spectrum ranging from 10 % to 90 %. The differential TOF between consecutive frequency bands was analyzed, which were subsequently subjected to absolute value transformation and visualized for analysis, as presented in Fig. 4(a-d).

The rationale for employing frequency bands rather than discrete frequencies stems from the understanding that analyzing frequency segments can provide a more robust characterization of acoustic behavior across diverse moisture levels, enhancing measurement fidelity and resilience against interference. This approach promotes the attainment of optimal TOF differentials that are sensitive to moisture variations under a range of conditions (Wotzka and Zmarzly, 2024). Based on the previously defined precision criteria, when the absolute differential

TOF between adjacent frequency bands falls within the 1 ns tolerance (reflecting the target precision), the bands are deemed to offer comparable discriminatory power for MC.

As shown in Fig. 4(c), for a container distance of 8 cm, the absolute differential TOF values for both the 40–60 kHz and 60–80 kHz bands predominantly reside within the 1 ns threshold. This observation suggests that, at this distance, these frequency bands possess sufficient sensitivity to effectively capture the range of TOF variations induced by changes in sludge MC. Considering the practical advantages associated with lower frequencies—namely, reduced attenuation that facilitates effective penetration through sludge and potentially lower instrumentation costs—this investigation advocates for selecting the 40 kHz emission frequency coupled with a container distance of 8 cm as the preferred configuration. Furthermore, analysis of Fig. 4(d) indicates that the combination of 80 kHz and a 10 cm container distance represents another viable option. Conversely, for the shorter container distances of 4 cm and 6 cm, the differential TOF consistently exceeded the 1 ns benchmark across adjacent frequency bands, indicating suboptimal performance at these configurations.

Synthesizing the simulation analysis, two viable parameter configurations were identified: 40 kHz coupled with an 8 cm container distance and 80 kHz paired with a 10 cm container distance. Both demonstrated the capacity to effectively capture the range of TOF variations attributable to fluctuations in MC, exhibiting commendable sensitivity. However, in the subsequent process of selecting the optimal scheme, a more thorough deliberation was undertaken. While both configurations demonstrated feasibility within the simulation framework, it is crucial to acknowledge that sludge is a complex medium characterized by significant acoustic attenuation. Lower-frequency ultrasound inherently possesses superior penetration capabilities and experiences reduced intrinsic attenuation. Consequently, the 40 kHz signal incurs comparatively lower energy dissipation during its transit through the sludge. This advantage facilitates more effective penetration across the 8 cm distance, particularly in scenarios involving higher sludge consistency or significant heterogeneity, ultimately yielding superior received signal strength and an enhanced SNR. Achieving robust SNR is paramount for precise and stable TOF measurements. Furthermore, 40 kHz represents a standard industrial frequency band, benefiting from mature and cost-effective transducer technology. Systems operating at this frequency typically exhibit relatively lower power consumption, which positively impacts the practical construction and long-term sustainability of the detection system. Integrating these discernible advantages related to both signal propagation fidelity and engineering economics, this study designates the configuration employing a 40 kHz emission frequency and an 8 cm container distance as the preferred operational scheme. This selection aims to establish a sludge MC detection system that is robust in performance while remaining economically viable.

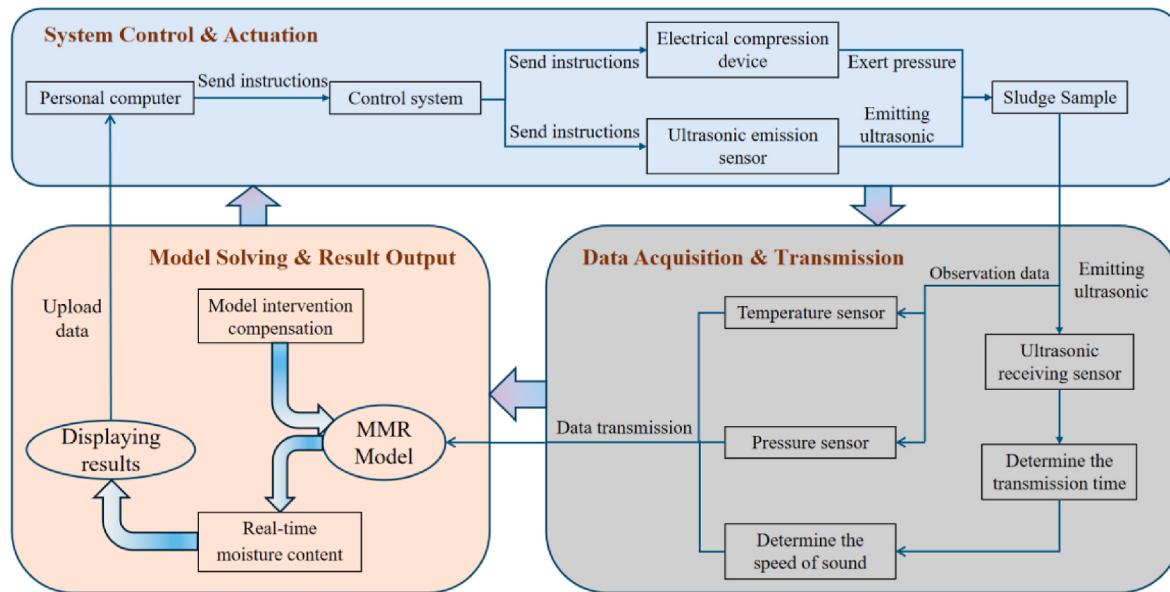
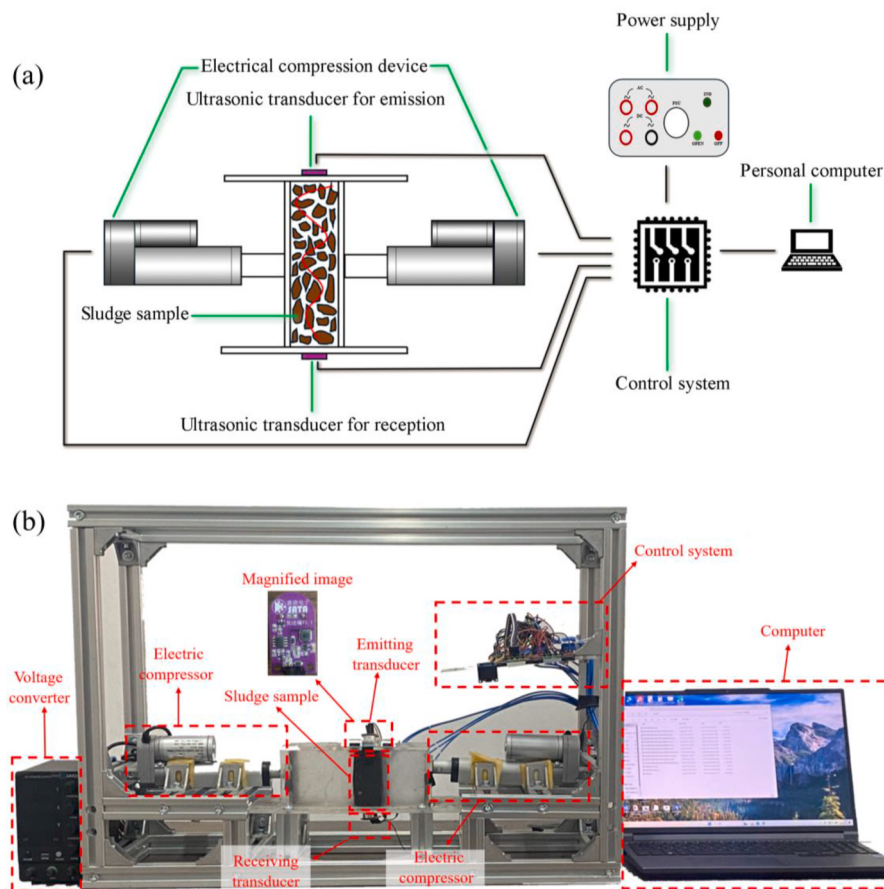
### 2.3. Sludge samples

Sludge samples for this investigation were collected from the Qige Wastewater Treatment Plant located in Hangzhou, Zhejiang Province, China. This facility employs an anaerobic-anoxic-oxic (AAO) process for the effective removal of nitrogen and phosphorus from municipal wastewater. After being collected, these raw sludge samples underwent initial treatment involving flocculation, induced by the addition of polyacrylamide (PAM) as a flocculant, followed by pre-dewatering using a belt press filter. The resultant pre-dewatered sludge, with an initial MC ranging from approximately 80 %–85 %, constituted the primary material for subsequent experimentation. To generate samples with varying MC, aliquots of the pre-dewatered sludge were placed in suitable containers and subjected to controlled drying in an oven maintained at a constant temperature of 105 °C. The duration of the heating cycle was carefully controlled to regulate the extent of moisture reduction. Upon completion of each heating period, the sludge samples were allowed to

**Table 1**

Physico-chemical characteristics and fundamental parameters of the sludge samples.

| Moisture content(%) | pH         | VSS/SS (%) | Carbon (%)  | Hydrogen (%) | Oxygen (%)   | Nitrogen (%) |
|---------------------|------------|------------|-------------|--------------|--------------|--------------|
| 10–90               | 6.9 ± 0.02 | 61.24      | 28.7 ± 0.02 | 4.46 ± 0.02  | 15.15 ± 0.02 | 4.34 ± 0.02  |

**Fig. 5.** Process flow diagram of the device.**Fig. 6.** (a) Schematic diagram of the ultrasonic transmission detection system; (b) Photograph of the actual experimental setup.

**Table 2**

List of components.

| No. | Item                     | Specification                                                   | Quantity |
|-----|--------------------------|-----------------------------------------------------------------|----------|
| 1   | Electric linear actuator | Power supply type:DC motor<br>Stroke range:200 mm               | 2        |
| 2   | Ultrasonic transmitter   | Detection accuracy:0.1 cm<br>Frequency:40 kHz/±50 Hz            | 1        |
| 3   | Ultrasonic receiver      | Detection accuracy:0.1 cm<br>Frequency:40 kHz/±50 Hz            | 1        |
| 4   | Variable DC power supply | Output range:0~30 V/0~5 A<br>Input voltage:220 V ± 10%/50 Hz    | 1        |
| 5   | Main controller          | Model:STM32F103C8T6                                             | 1        |
| 6   | Relay                    | Maximum load:<br>AC 250 V/10 A DC 30 V/10 A                     | 4        |
| 7   | Pressure sensor          | Sensitivity:1.5 mV/V                                            | 2        |
| 8   | Load cell                | Measurement range:0~10 kg<br>Calibration accuracy:±1 g          | 1        |
| 9   | Temperature sensor       | Temperature range: 70~550 °C<br>Tolerance class:±2.5 °C/±0.75 % | 1        |
| 10  | OLED display             | Resolution:128*64<br>Interface type:SPI interface               | 1        |
| 11  | Button                   | -                                                               | 2        |

equilibrate to ambient temperature, after which their precise mass was recorded. This systematic procedure facilitated the preparation of a series of sludge samples with distinct, predetermined MC levels. Concurrently, the actual MC of each prepared sample was accurately calculated using Eq. (8), providing essential quantitative data crucial for the subsequent experimental phases. Key properties of the sludge samples used in this study are summarized in Table 1. To prevent sample degradation and subsequent alterations in physicochemical characteristics, all prepared samples were stored under refrigeration at 4 °C and used within a maximum of 3 days post-preparation.

$$M_c = \frac{W_s - W_d}{W_s} \times 100\% \quad (8)$$

Where  $M_c$  is the MC of sludge (%),  $W_s$  is the mass of the original sludge (g), and  $W_d$  is the mass of sludge after drying at 105 °C for 24 h (g).

#### 2.4. Experimental apparatus

Fig. 5 illustrates the workflow of the system. The experimental workflow begins with the control system sending instructions from a host computer to both the electrical compression device and the ultrasonic emission sensor. Upon receiving the control signal, the compression device initially applies the designated pressure to the sludge sample. Once compression is completed, the ultrasonic emission sensor subsequently transmits sound waves through the sample. On the receiving end, the ultrasonic sensor detects the transmitted signal and calculates the sound transmission time, from which the speed of sound through the sludge is determined. In parallel, embedded temperature and pressure sensors acquire real-time environmental data. These observation data are transmitted to the MMR model for integrated analysis. The model performs compensation based on system conditions and computes the real-time MC of the sludge. The results are then output to the display interface for detection and logging. This procedure ensures that all sensing, actuation, and computational processes are synchronized within a closed-loop system, enabling accurate and efficient MC. The primary instruments used in this experimental investigation included an electronic balance (sensitivity: 0.001 g), a drying oven, porcelain dishes, ultrasonic transducers (operational frequency range: 0.5–1.5 MHz), a motorized compression unit, a dedicated control system, a power supply unit, and a host computer. A schematic diagram illustrating the configuration of the experimental apparatus is shown in Fig. 6(a). To provide a clearer illustration of the composition of the experimental apparatus, Table 2 presents a detailed inventory of its constituent components, facilitating the reader's comprehension of the

**Table 3**

Correlation between sludge physical state variation at different MC and the relevance of bulk density.

| Moisture content(%) | Sludge physical state | Bulk density relevance |
|---------------------|-----------------------|------------------------|
| Above 55            | Semi-liquid           | Disregarded            |
| 55 to 24            | Clay-like             | Relevant               |
| Below 24            | Hardened              | Disregarded            |

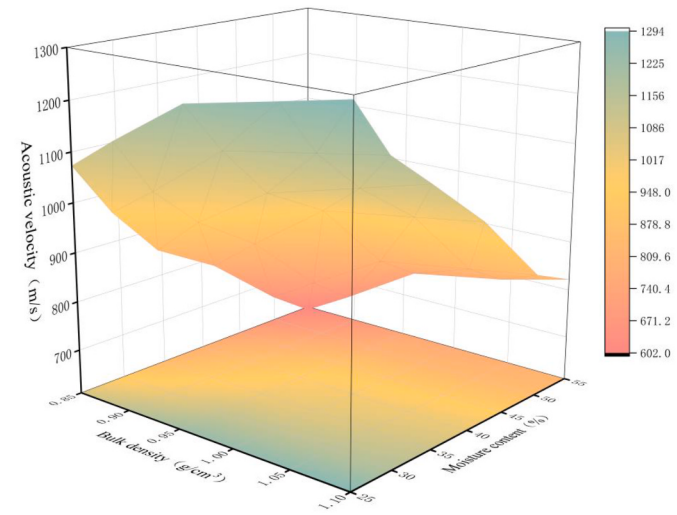


Fig. 7. Relationship between bulk density and acoustic velocity across various MC.

specific device structure. A photograph of the actual experimental setup is shown in Fig. 6(b).

### 3. Results and discussion

#### 3.1. Analysis of factors influencing MC

Variations in sludge MC are influenced by multiple factors, including its intrinsic composition, physical properties, and prevailing environmental conditions. In this context, the present investigation will focus on elucidating the influence of two specific factors: bulk density and temperature.

##### 3.1.1. Influence of bulk density

The porosity of sludge significantly influences the distribution and migration dynamics of its internal moisture. Specifically, the pore architecture governs the retention characteristics of interstitial and capillary water fractions within the sludge matrix, thus impacting the accuracy of MC determination (Wang et al., 2024). Therefore, elucidating the correlation between porosity and MC is crucial for optimizing dewatering efficacy and enabling precise characterization of sludge properties. However, the prevalence of inaccessible (closed) pores within the sludge structure, combined with constraints preventing destructive sampling during in-situ measurements, necessitates the use of surrogate parameters. To this end, this study adopted bulk density (mass per unit volume) as a relevant indicator. Table 3 shows the relationship between sludge variations at different MC and its bulk density. At MC exceeding 55 %, applied compressive stress facilitates the formation of free water films between particles, creating a lubricating effect that promotes inter-particle slippage. Consequently, under these conditions, the bulk density of high-moisture sludge becomes less representative of its intrinsic structural arrangement due to particle rearrangement facilitated by lubrication (Wang et al., 2016). Conversely, at MC below 24 %, inter-particle contacts become

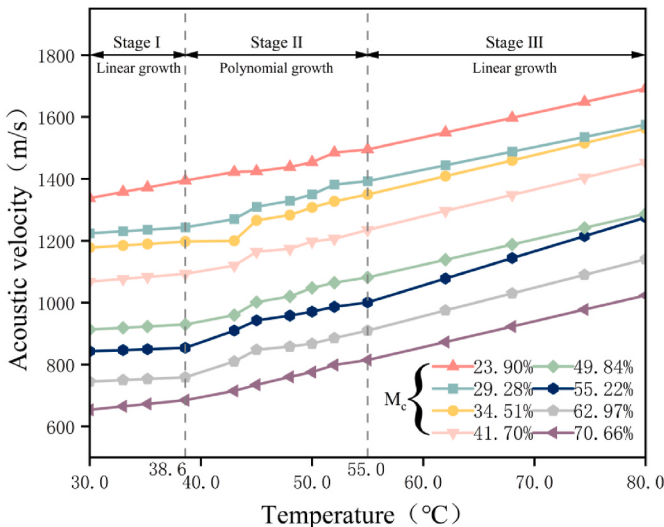


**Fig. 8.** Relationship between temperature and acoustic velocity at various MC.

significantly consolidated, with negligible lubricating water films present. This state makes further compaction and reduction in porosity challenging. As such, the bulk density of low-moisture sludge also shows limited sensitivity to structural variations, approaching a state of maximum compaction (Latońska et al., 2021). Based on this analysis, the effective range for using bulk density as an indicative parameter of sludge structure related to moisture retention was determined to be 24%–55% MC.

To elucidate the influence of bulk density relevant to this investigation, the relationship between bulk density and acoustic velocity was systematically examined across a spectrum of sludge MC (ranging from 23.90 % to 55.22 %), with the findings presented in Fig. 7. Each data point presented herein represents the arithmetic mean derived from five independent measurements conducted per sample, a methodological approach used to ensure the precision and reliability of the results. As illustrated in Fig. 7, acoustic velocity is significantly influenced by both bulk density and MC variations. The overarching trend indicates that, within the experimental range explored, acoustic velocity exhibits a positive correlation with bulk density; Specifically, increases in bulk density correspond to increases in acoustic velocity. Conversely, a negative correlation exists between acoustic velocity and MC, indicating that higher moisture levels lead to reduced acoustic velocity. Consequently, the maximum observed acoustic velocity occurs under conditions of high bulk density combined with low MC, while the minimum velocity is recorded at low bulk density and high MC. This pattern clearly highlights the combined influence of sludge compactness and hydration level on the acoustic propagation characteristics within the material.

### 3.1.2. Influence of temperature

When employing ultrasonic techniques to determine sludge MC, the influence of temperature primarily manifests in three critical aspects. Firstly, elevated temperatures accelerate moisture evaporation and modulate water activity, thereby introducing a potential discrepancy between the in-situ MC of the sludge and its condition during measurement (Wang et al., 2021). Secondly, thermal variations can induce significant changes in the physico-chemical properties of the sludge. These modifications include phenomena such as particle expansion, decomposition of organic constituents, and transformations in the pore architecture. Furthermore, temperature shifts can weaken inter-particle binding forces and promote aggregation, thereby disrupting the inherent structural integrity of the sludge (Zhi et al., 2024). Lastly, fluctuations in ambient temperature may affect the performance stability of the ultrasonic sensors themselves. Concurrently, intensified vibrations of sludge

particles and increased molecular thermal motion alter the attenuation patterns of ultrasonic waves propagating through the medium. This perturbation can consequently invalidate MC calculations based on acoustic attenuation models, leading to inaccurate results (Wen et al., 2024). Therefore, meticulous consideration of thermal effects and the implementation of necessary compensatory strategies during the detection process are imperative to ensure measurement fidelity.

Fig. 8 illustrates the relationship between temperature and acoustic velocity at various sludge MC. Each data point plotted represents the arithmetic mean derived from five independent measurements conducted on each sample, a methodology used to ensure the accuracy and reliability of the results. It is evident that within the temperature range of 30.0 °C–38.6 °C, acoustic velocity exhibits a positive linear correlation with increasing temperature. This trend can be plausibly attributed to the fact that within this thermal regime, substantial internal moisture evaporation has not yet been significantly activated, thereby maintaining relatively stable inter-particle contact interfaces (Kim et al., 2016). However, as the temperature rises into the 38.6 °C–55.0 °C range, the previously linear growth trajectory transitions into a polynomial trend. This shift closely coincides with the dynamic equilibrium between moisture evaporation and retention in the sludge reaching a critical point or peak. During this phase, the sludge likely undergoes dynamic reconfiguration of its pore structure, accompanied by increased fluctuations in its elastic modulus. These concurrent changes are believed to induce a more complex, non-linear response in acoustic propagation, potentially reflected in variations in attenuation characteristics or in the rate of change of velocity, thus deviating from the simpler linear behavior observed previously (Liu et al., 2023). Subsequently, when the temperature exceeds 55.0 °C, the growth trend of acoustic velocity reverts to a linear pattern. This latter linear increase is likely attributable to the sustained high temperatures inducing hardening or stiffening of the sludge skeletal matrix, which leads to the compression of inter-particle voids into a relatively stable, consolidated state (Xu et al., 2019).

### 3.2. Hybrid prediction model construction

A dataset was generated through experimental investigations, and the measurement results were subsequently evaluated using a gross error treatment methodology. Following the systematic elimination of identified outliers (gross errors), a refined dataset comprising 130 validated data points was established, correlating actual sludge MC with the corresponding predictor variables. To elucidate the potential underlying relationships among the variables in this curated experimental data, MLR analysis was employed as a preliminary modeling approach. Within this framework, temperature, bulk density, and acoustic velocity were defined as independent variables (predictors), while MC served as the dependent variable (response). The refined experimental data were fitted using this regression technique, resulting in the derivation of Regression Eq. (9).

$$y = 0.95 + 5.55 \times 10^{-3} x_1 + 1.27 \times x_2 - 6.83 \times 10^{-4} x_3 \quad (9)$$

Where,  $x_1$  represents the temperature in degrees Celsius (°C),  $x_2$  denotes the bulk density in grams per cubic centimeter (g/cm<sup>3</sup>),  $x_3$  signifies the acoustic velocity in meters per second (m/s), and  $y$  corresponds to the MC expressed as a percentage (%).

To ascertain the congruence between the regression equation and the empirical data, this study used the achieving a coefficient of determination ( $R^2$ ), a standard metric in regression analysis for evaluating goodness-of-fit. Based on statistical evaluation, the  $R^2$  value for this MLR model was found to be 0.891. Being close to unity, this value suggests a commendable overall predictive capability of the MLR model in capturing the general variance within the dataset. However, a high  $R^2$  value, while indicative of the model's proficiency in explaining global data trends, does not guarantee superior predictive precision. It may

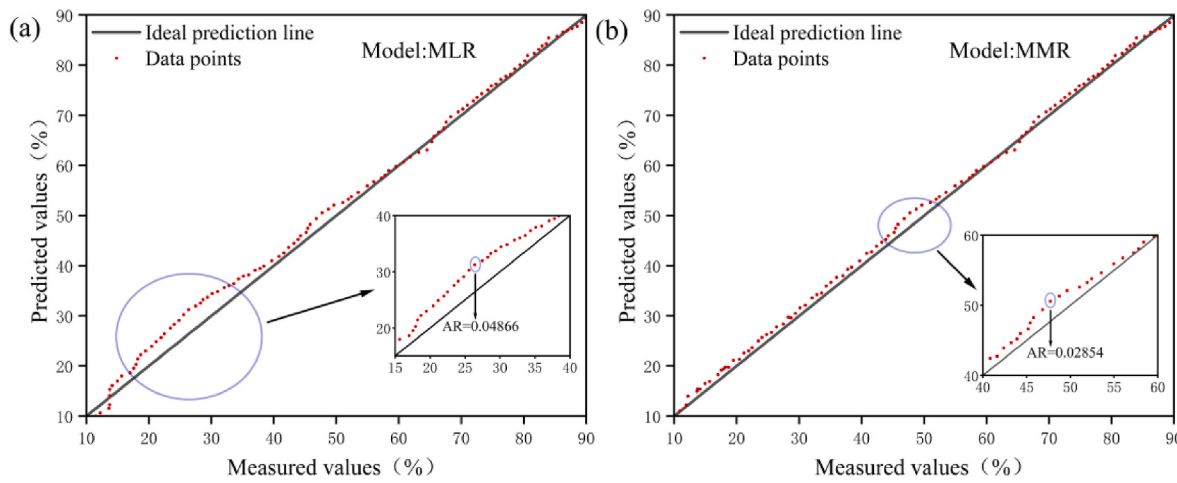


**Fig. 9.** Scatter plots comparing experimental versus predicted MC values for (a) the MLR model and (b) the MMR model.

obscure localized data characteristics or fail to adequately account for outliers. Consequently, to more rigorously evaluate the model's predictive fidelity, a scatter plot comparing the experimentally observed values with the model-predicted values was generated, as depicted in Fig. 9(a). Inspection of Fig. 9(a) reveals instances of suboptimal concordance for certain data points, evidenced by a maximum absolute residual (AR) of 0.04866. This observation highlights the limitations of the MLR model in fully capturing the inherent non-linear relationships within the data. Furthermore, considering the previously identified polynomial growth trend associated with the temperature variable during the experimental phase, it is evident that, despite including temperature as a predictor, the model requires refinement through the integration of non-linear components to more accurately reflect the complex interplay of variables, particularly the nuanced influence of temperature.

Interaction terms in multiple non-linear regression models refer to the explicit incorporation of terms that represent the combined effects or interplay between independent variables. The primary rationale for introducing these terms is to effectively capture non-linear relationships, particularly scenarios where the influence of one predictor on the dependent variable depends on the level of another predictor. By integrating these interaction effects, the model gains enhanced flexibility and the capacity to more accurately represent the underlying data structure, thereby improving the overall goodness-of-fit, especially when substantial interdependencies exist among the predictors. In the context of this investigation, temperature, bulk density, and acoustic velocity were designated as independent variables (predictors), while MC served as the dependent variable (response). The application of this non-linear regression approach, which incorporates relevant interaction terms, resulted in the formulation of Regression Eq. (10).

$$y = \beta_0 + \beta_1 x_1 + \dots + \beta_m x_m + \sum_{1 < j < k < m} \beta_{jk} x_{jk} + \varepsilon \quad (10)$$

Where,  $x_m$  denotes the accurately measured and controllable independent variable,  $y$  represents the dependent (response) variable, and  $\varepsilon$  is the random error term.

To more effectively capture the influence of temperature variations on the model's predictive accuracy, particularly in addressing the previously identified non-linear behavior within a specific thermal range, this study implemented a segmented modeling strategy. The dataset was partitioned into three distinct temperature intervals. Specifically, for the intermediate temperature range, a multiple non-linear regression model was used; This model strategically incorporated interaction terms to better represent the complex non-linear dependencies observed within this segment. Conversely, for the lower and upper temperature ranges, the analysis utilized multiple linear regression equations, which were

**Table 4**

Regression equations for the MMR model within specified temperature intervals.

| Temperature interval | Regression equation                                                                                                                                                                                                         |
|----------------------|-----------------------------------------------------------------------------------------------------------------------------------------------------------------------------------------------------------------------------|
| 30.0°C–38.6 °C       | $y_1 = 0.76 + 0.75 \times 10^{-3} x_1 + 0.08 x_2 - 0.61 \times 10^{-4} x_3$                                                                                                                                                 |
| 38.6°C–55.0 °C       | $y_2 = 2.05 - 0.02 x_1 + 0.05 x_2 - 0.13 \times 10^{-3} x_3 + 0.37 \times 10^{-4} x_1^2 - 0.11 x_2^2 + 3.45 \times 10^{-7} x_3^2 - 3.92 \times 10^{-4} x_1 x_2 - 4.49 \times 10^{-6} x_1 x_3 + 8.16 \times 10^{-5} x_2 x_3$ |
| 55.0°C–80.0 °C       | $y_3 = 1.36 + 2.99 \times 10^{-3} x_1 - 0.12 x_2 - 7.57 \times 10^{-4} x_3$                                                                                                                                                 |

considered suitable for characterizing the relationships in these regimes. This piecewise approach yielded a refined set of regression equations tailored to each specific temperature interval, as detailed in Table 4.

To rigorously assess the predictive performance of the developed MMR model, the refined dataset (post-outlier treatment), comprising 130 pairs of actual sludge MC values and their corresponding model-predicted values, was utilized. Computational analysis yielded an  $R^2$  of 0.964 for the MMR model. This value signifies a substantial enhancement compared to the initial linear model, which can be directly attributed to the strategic incorporation of interaction terms within the specific temperature interval previously identified as exhibiting a polynomial growth trend. Consistent with the evaluation methodology employed earlier, a scatter plot correlating the experimentally observed values with the MMR model predictions was generated to visually assess the model's predictive fidelity, as presented in Fig. 9(b). An examination of Fig. 9(b) unequivocally demonstrates a significant improvement in the goodness of fit, with a noticeably tighter clustering of data points around the line of perfect agreement. This enhanced concordance is quantitatively supported by a reduction in the maximum AR to 0.02854, thereby underscoring the superior accuracy and reliability of the proposed MMR model.

### 3.3. Model comparison and evaluation

To facilitate a scientific comparison of the MMR model's performance, this study introduces a backpropagation neural network (BPNN) to construct a nonlinear mapping model. Temperature, bulk density, and sound velocity serve as input variables, while sludge MC is designated as the output variable. To ensure a fair comparison between models, both BPNN and MMR employ identical training and validation datasets, with a 7:3 train-validation split. Prior to input into the neural network, all data are normalized to mitigate the impact of dimensional disparities—particularly between sound velocity and other variables—on computational accuracy. The architecture of the BPNN is defined by specifying the number of network layers, selecting the number of hidden

**Table 5**  
Comparative performance evaluation of the two regression models.

| Model | R <sup>2</sup> | MAE   | RMSE  |
|-------|----------------|-------|-------|
| MLR   | 0.873          | 4.196 | 5.373 |
| BPNN  | 0.886          | 4.036 | 5.093 |
| MMR   | 0.978          | 1.901 | 2.233 |

nodes, configuring the activation function, and choosing an appropriate training algorithm. To balance computational efficiency with model accuracy, the constructed BPNN comprises three layers: input, hidden,

and output. The number of nodes in the input and output layers is determined by model characteristics and prediction objectives, and is therefore set to 3 and 1, respectively. The number of hidden layer nodes is selected based on empirical formulas and further refined through performance optimization. The recommended range for hidden nodes is between 3 and 12(Huang et al., 2023). Under fixed values for other parameters, various hidden node counts are tested, and their corresponding mean square errors (MSE) are compared. Ultimately, the number of hidden nodes is set to 10, corresponding to the lowest MSE and indicating optimal model performance.

To comprehensively assess the predictive capabilities of the three

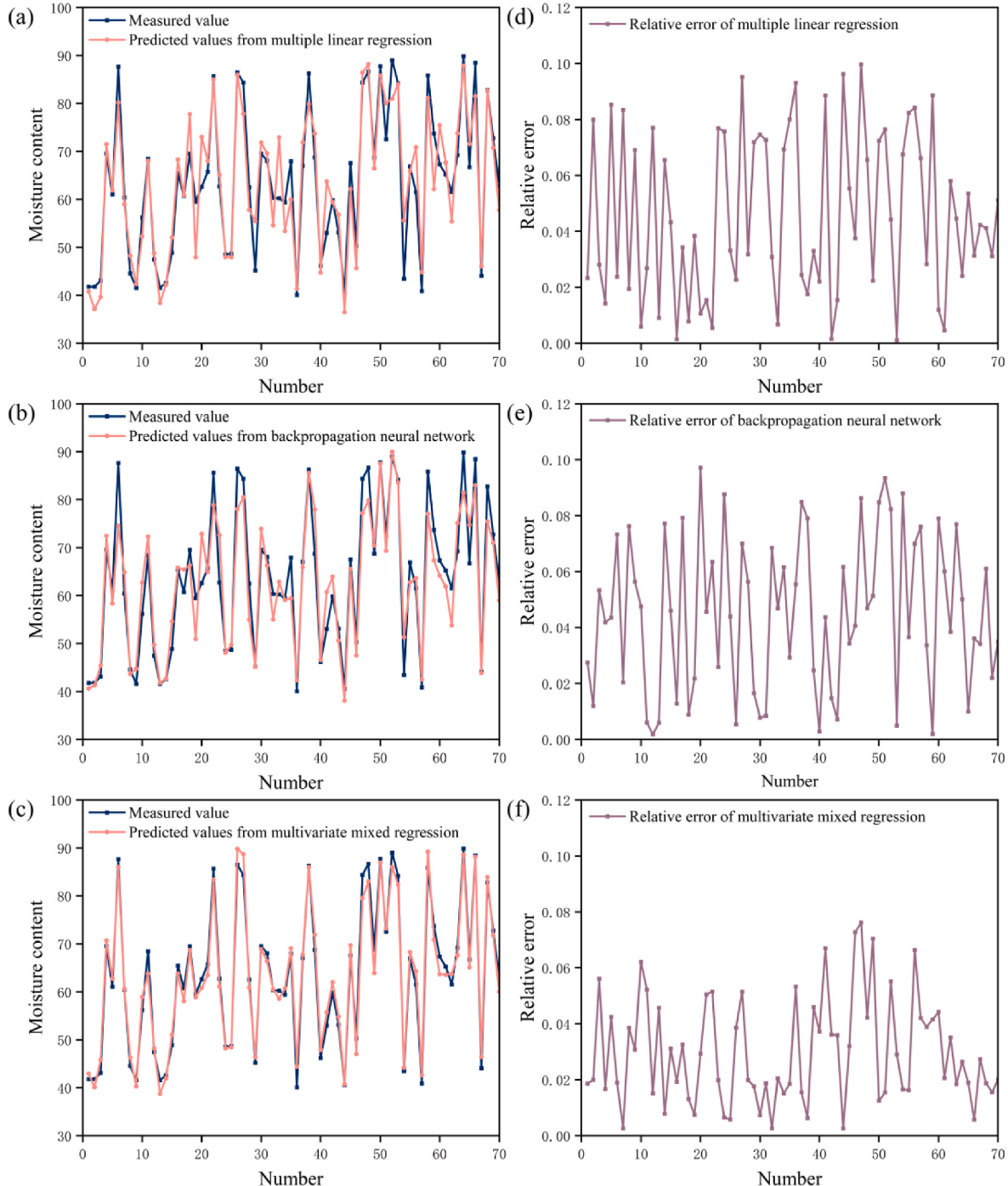


**Fig. 10.** (a) Comparison plot of experimental versus predicted values for the MLR model; (b) Comparison plot of experimental versus predicted values for the BPNN model; (c) Comparison plot of experimental versus predicted values for the MMR model; (d) Relative error plot for the MLR model; (e) Relative error plot for the BPNN model; (f) Relative error plot for the MMR model.

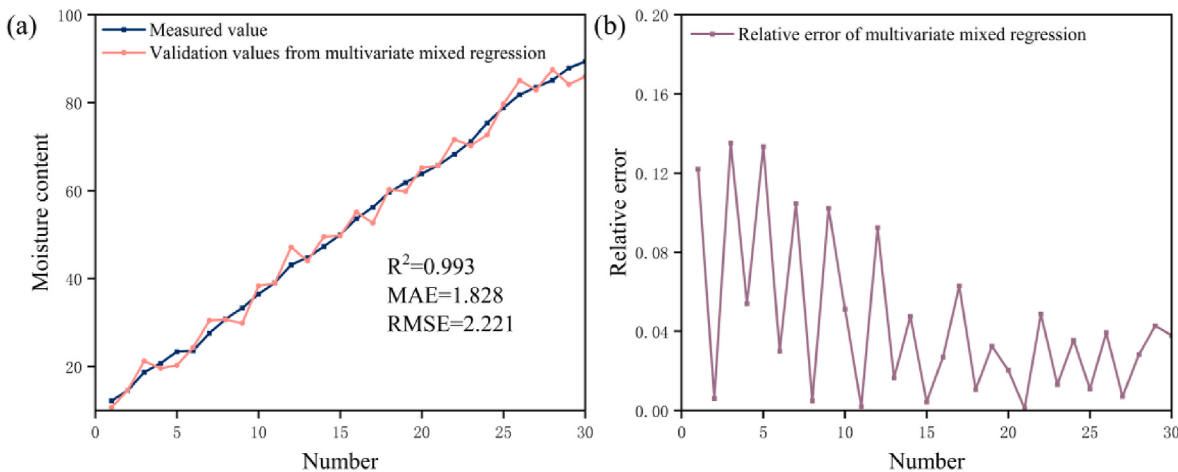


**Fig. 11.** (a) Comparison plot of experimental and validation values for the MMR model; (b) Relative error plot for the MMR model.

developed models, this study employed the  $R^2$ , the mean absolute error (MAE) and the root mean square error (RMSE) as key evaluation metrics to compare the performance of the MLR, BPNN, and MMR models. Detailed results are presented in Table 5. The data in Table 5 indicate that the MMR model outperformed the other two models across all three statistical metrics. Additionally, to quantify the relative differences between experimental observations and model predictions, relative error (RE) was incorporated into the evaluation framework. Model prediction accuracy was further validated using a dataset of 70 processed samples. Fig. 10(a)–10(c) provide a visual comparison between experimental measurements and model predictions. Fig. 10(d)–10(f) illustrate the distribution of the corresponding relative error values. A detailed analysis of Fig. 10(d)–10(f) reveals that the RE values of the MMR model are consistently lower than those of the other two models. This finding offers empirical evidence supporting the MMR model's superior ability to capture complex nonlinear interactions among input variables. Based on this comprehensive analysis, the MMR model was ultimately selected as the preferred method for correcting the original output of the detection device, aiming to enhance predictive accuracy in practical engineering applications.

### 3.4. Method validation and outlook

To further assess the generalizability and robustness of the proposed MMR model, an independent validation experiment was conducted using 30 municipal sludge samples collected from a different wastewater treatment facility operated by the Yiwu Water Affairs Construction Group in Zhejiang Province. The model's predictive performance was evaluated using four commonly adopted statistical metrics:  $R^2$ , the MAE, the RMSE and the RE. The MMR model maintained consistently high predictive performance on this new dataset, achieving an  $R^2$  of 0.993, MAE of 1.828 and RMSE of 2.221, as shown in Fig. 11(a). The RE results are illustrated in Fig. 11(b). These results demonstrate that the model is not overly dependent on a specific sludge source and can effectively accommodate variations in sludge properties, thereby reinforcing its applicability and reliability across diverse treatment conditions.

Despite its promising performance, this study has several notable limitations. The current model is primarily data-driven and lacks a mechanistic explanation of how ultrasonic wave propagation is affected by sludge microstructure, including factors such as extracellular polymeric substances and particle morphology. Second, the dataset used for model training and validation, while representative, is limited in scope and does not capture the full range of sludge types and dewatering conditions encountered in real-world applications. Additionally, the long-term performance and operational stability of the developed system in field conditions require further validation. Future research should

aim to enhance the model's physical interpretability by integrating detailed characterizations of sludge microstructure and composition. Multi-source data fusion and advanced modeling strategies could further improve the model's adaptability to diverse sludge types and treatment processes. Moreover, further efforts are needed to verify the system's robustness under diverse environmental conditions and to develop a generalized framework for full-scale industrial deployment.

## 4. Conclusions

This study proposes and validates an innovative method that integrates ultrasonic transmission technology with the MMR model, providing a rapid, non-destructive, precise, and stable and reliable online MC detection scheme for the real-time optimization control of municipal sludge dewatering process. Based on simulation optimization and comprehensive engineering economic evaluation, a dedicated experimental device integrating adaptive bulk density correction and embedded temperature compensation functions was developed, providing accurate input features for the MMR model and ensuring its superior predictive performance. The main conclusions are as follows: (1) The identification of effective acoustic measurement parameters (40 kHz emission frequency, 8 cm container distance) through COMSOL simulations and experimental validation, balancing performance with cost-efficiency. A dedicated device featuring adaptive bulk density correction and embedded temperature compensation was engineered and achieved sub-15-s measurement cycles. Applying the MMR model to ultrasonic MC detection yielded superior accuracy: versus MLR and BPNN models, its  $R^2$  increased by 12.08 % and 10.37 %, MAE decreased by 54.71 % and 52.91 %, and RMSE decreased by 58.44 % and 56.16 %. (2) Although these advances are promising, the study still has certain limitations. The MMR model's predictive strength is primarily data-driven, lacking a clear physical explanation of how ultrasonic wave propagation interacts with key sludge microstructural elements. Furthermore, the dataset, while representative, was limited in scope regarding sludge variability and dewatering scenarios encountered in full-scale operations. The long-term robustness and stability of the system under diverse, real-world field conditions also remain to be fully assessed. (3) Future research should focus on enhancing the model's physical interpretability by integrating detailed analyses of sludge microphysical properties to elucidate the fundamental links between ultrasonic signal responses and sludge state. Expanding model adaptability will require multi-source data fusion techniques and advanced modeling strategies tailored to a wider array of sludge types and treatment processes. Crucially, rigorous validation of the system's operational resilience across varied environmental conditions is essential, paving the way for the development of a generalized framework suitable

for industrial-scale implementation.

## CRediT authorship contribution statement

**Yan Zhang:** Writing – original draft, Methodology, Investigation, Conceptualization. **Zhichao Zheng:** Writing – original draft, Visualization, Supervision, Resources, Methodology, Investigation, Data curation, Conceptualization. **Fudong Gong:** Writing – review & editing, Visualization, Resources. **Shu Cheng:** Writing – original draft, Software, Methodology. **Hao Xu:** Writing – original draft, Methodology, Data curation. **Zhongzhong Zhang:** Resources, Funding acquisition. **Yawen Yao:** Methodology, Funding acquisition, Conceptualization. **Binqi Rao:** Writing – review & editing, Writing – original draft, Project administration, Funding acquisition, Formal analysis, Conceptualization.

## Declaration of competing interest

The authors declare that they have no known competing financial interests or personal relationships that could have appeared to influence the work reported in this paper.

## Acknowledgments

The authors gratefully acknowledge the financial support from Zhejiang Provincial Natural Science Foundation (LZ23E080001, LZ24E060002), National Natural Science Foundation of China (grant numbers 52376079), The Key Research and Development Program of Zhejiang Province (2024C03138), Major Scientific Research Projects of Jinhua City (2023–1–002).

## Data availability

Data will be made available on request.

## References

- An, W., Wang, H., Yang, T., Xu, J., Wang, Y., Liu, D., Hu, J., Cui, W., Liang, Y., 2023. Enriched photocatalysis-Fenton synergistic degradation of organic pollutants and coking wastewater via surface oxygen vacancies over Fe-BiOBr composites. *Chem. Eng. J.* 451, 138653. <https://doi.org/10.1016/j.cej.2022.138653>.
- Brouwers, B., van Beeck, J., Meire, D., Lataire, E., 2022. Assessment of the potential of radiography and ultrasonography to record flow dynamics in cohesive sediments (mud). *Front. Earth Sci.* 10, 878102. <https://doi.org/10.3389/feart.2022.878102>.
- El Jery, A., Kosarirad, H., Taheri, N., Bagheri, M., Alderdery, M., Elkhaleefa, A., Wang, C., Sammen, S.S., 2023. An application of ultrasonic waves in the pretreatment of biological sludge in urban sewage and proposing an artificial neural network predictive model of concentration. *Sustainability* 15 (17). <https://doi.org/10.3390/su151712875>.
- Elvira, L., Vera, P., Cañadas, F.J., Shukla, S.K., Montero, F., 2016. Concentration measurement of yeast suspensions using high frequency ultrasound backscattering. *Ultrasonics* 64, 151–161. <https://doi.org/10.1016/j.ultras.2015.08.009>.
- Fan, J., Wang, F., Lv, G., Cui, H., Wang, W., 2023. Moisture content online measurement in the sludge by ultrasonic reflection method. *Phys. Scri.* 99 (1), 015006. <https://doi.org/10.1088/1402-4896/ad1086>.
- Gover, A.R., Kopiński, J., 2022. Higher fundamental forms of the conformal boundary of asymptotically de Sitter spacetimes. *Classical Quant. Grav.* 40 (1), 015001. <https://doi.org/10.1088/1361-6382/aca459>.
- Hong, W., Kun, W., Jing-zhu, W., Ping, H., 2021. Progress in research on rapid and non-destructive detection of seed quality based on spectroscopy and imaging technology. *Spectrosc. Spectr. Anal.* 41 (1), 52–59. [https://doi.org/10.3964/j.issn.1000-0593\(2021\)01-0052-08](https://doi.org/10.3964/j.issn.1000-0593(2021)01-0052-08).
- Huang, Z.R., Ge, M., Pang, X.R., Song, P., Wang, C., 2023. The spatial distribution of interleukin-4 (IL-4) reference values in China based on a back propagation (BP) neural network. *Geospat Health* 18 (2). [https://doi.org/10.3964/j.issn.1000-0593\(2021\)01-0052-08](https://doi.org/10.3964/j.issn.1000-0593(2021)01-0052-08).
- Jameel, B., Hornowski, T., Bielas, R., Józefczak, A., 2022. Ultrasound study of magnetic and non-magnetic nanoparticle agglomeration in high viscous media. *Materials* 15 (10), 3450. <https://doi.org/10.3390/ma15103450>.
- Jia, Y., Li, S., Ma, H., Gao, J., Zhu, G., Zhang, F., Park, J.Y., Cha, S., Bae, J.-S., Liu, C., 2020. Oxygen vacancy rich Bi2O4-Bi4O7-BiO2-x composites for UV-vis-NIR activated high efficient photocatalytic degradation of bisphenol A. *J. Hazard Mater.* 382, 121121. <https://doi.org/10.1016/j.jhazmat.2019.121121>.
- Kamalinia, H., Tie, B., 2023. Numerical and analytical studies of attenuation coefficient in 2D matrix-inclusion composites with randomly distributed circular inclusions. *Wave Motion* 123, 103225. <https://doi.org/10.1016/j.wavemoti.2023.103225>.
- Kim, M., Lee, Y., Park, J., Ryu, C., Ohm, T.-I., 2016. Partial oxidation of sewage sludge briquettes in a updraft fixed bed. *Waste Manag* 49, 204–211. <https://doi.org/10.1016/j.wasman.2016.01.040>.
- Latosińska, J., Żygała, M., Czapik, P., 2021. The influence of sewage sludge content and sintering temperature on selected properties of lightweight expanded clay aggregate. *Materials* 14 (12), 3363. <https://doi.org/10.3390/ma14123363>.
- Li, C., Yu, X., Chen, Z., Song, Q., Xu, Y., 2021. Free space traveling-standing wave attenuation method for microwave sensing of grain moisture content. *Measurement and Control* 54 (3–4), 336–345. <https://doi.org/10.1177/0020294020962138>.
- Li, C., Zhao, C., Ren, Y., He, X., Yu, X., Song, Q., 2022. Microwave traveling-standing wave method for density-independent detection of grain moisture content. *Measurement* 198, 111373. <https://doi.org/10.1016/j.measurement.2022.111373>.
- Li, X., Shen, X., Jiang, W., Xi, Y., Li, S., 2024. Comprehensive review of emerging contaminants: detection technologies, environmental impact, and management strategies. *Ecotoxicol. Environ. Saf.* 278, 116420. <https://doi.org/10.1016/j.ecoenv.2024.116420>.
- Lin, F., Li, J.-g., Chai, X.-S., Zhang, Z.-b., Liu, M., 2020. Determination of water distribution in sludge by a multiple headspace extraction analytical technique. *J. Chromatogr. A* 1628, 461449. <https://doi.org/10.1016/j.chroma.2020.461449>.
- Liu, H., Maghoul, P., Shalaby, A., Thomson, D., 2023. Ultrasonic characterization of frozen soils using a multiphase poromechanical approach. *Comput. Geotech.* 153, 105068. <https://doi.org/10.1016/j.compgeo.2022.105068>.
- Liu, Z., Luo, F., He, L., Wang, S., Wu, Y., Chen, Z., 2024. Physical conditioning methods for sludge deep dewatering: a critical review. *J. Environ. Manag.* 360, 121207. <https://doi.org/10.1016/j.jenvman.2024.121207>.
- Liu, Z., Zhang, R., Yang, C., Hu, B., Luo, X., Li, Y., Dong, C., 2022. Research on moisture content detection method during green tea processing based on machine vision and near-infrared spectroscopy technology. *Spectrochim. Acta Mol. Biomol. Spectrosc.* 271, 120921. <https://doi.org/10.1016/j.saa.2022.120921>.
- Louisnard, O., 2012. A simple model of ultrasound propagation in a cavitating liquid. Part I: theory, nonlinear attenuation and traveling wave generation. *Ultrason. Sonochem.* 19 (1), 56–65. <https://doi.org/10.1016/j.ulsonch.2011.06.007>.
- Mazurek, K., Drużyński, S., Kielkowska, U., Węgrzynowicz, A., Nowak, A.K., Wzorek, Z., Wróbel-Kaszanek, A., 2023. Municipal sewage sludge as a source for obtaining efficient biosorbents: analysis of pyrolysis products and adsorption tests. *Materials* 16 (7), 2648. <https://doi.org/10.3390/ma16072648>.
- Nguyen, V.K., Chaudhary, D.K., Dahal, R.H., Trinh, N.H., Kim, J., Chang, S.W., Hong, Y., La, D.D., Nguyen, X.C., Ngo, H.H., 2021. Review on pretreatment techniques to improve anaerobic digestion of sewage sludge. *Fuel* 285, 119105. <https://doi.org/10.1016/j.fuel.2020.119105>.
- Okazaki, S., Iwase, H., Nakagawa, H., Yoshida, H., Hinai, R., 2021. Effect of moisture distribution on velocity and waveform of ultrasonic-wave propagation in mortar. *Materials* 14 (4), 790. <https://doi.org/10.3390/ma14040790>.
- Pilli, S., Bhunia, P., Yan, S., LeBlanc, R., Tyagi, R., Surampalli, R., 2011. Ultrasonic pretreatment of sludge: a review. *Ultrason. Sonochem.* 18 (1), 1–18. <https://doi.org/10.1016/j.ulsonch.2010.02.014>.
- Qi, Y., Chen, J., Xu, H., Wu, S., Yang, Z., Zhou, A., Hao, Y., 2024. Optimizing sludge dewatering efficiency with ultrasonic treatment: insights into parameters, effects, and microstructural changes. *Ultrason. Sonochem.* 102, 106736. <https://doi.org/10.1016/j.ulsonch.2023.106736>.
- Ruiz-Hernando, M., Vinardell, S., Labanda, J., Llorens, J., 2022. Effect of ultrasonication on waste activated sludge rheological properties and process economics. *Water Res.* 208, 117855. <https://doi.org/10.1016/j.watres.2021.117855>.
- Shao, A., Chu, J., 2023. Design and Research of an Ultrasonic Grain Moisture Content Detection Device. <https://doi.org/10.1109/IMCEC51613.2021.9482332>.
- Tang, Y., Zhang, P., Zhu, M., Li, J., Li, Y., Wang, Z., Huang, L., 2019. Temperature effects on the dielectric properties and breakdown performance of h-BN/epoxy composites. *Materials* 12 (24), 4112. <https://doi.org/10.3390/ma12244112>.
- Wang, B., Xu, Z., Dong, B., 2024. Occurrence, fate, and ecological risk of antibiotics in wastewater treatment plants in China: a review. *J. Hazard Mater.* 133925. <https://doi.org/10.1016/j.jhazmat.2024.133925>.
- Wang, G., Wang, S., Li, J., Chen, X., Qin, C., Ju, S., 2022. Experimental research on propagation and attenuation of ultrasonic waves in water-bearing coal. *Fuel* 324, 124533. <https://doi.org/10.1016/j.fuel.2022.124533>.
- van den Wildenberg, S., Jia, X., Roche, O., 2020. Acoustic probing of the particle concentration in turbulent granular suspensions in air. *Sci. Rep.* 10 (1), 16544. <https://doi.org/10.1038/s41598-020-73427-z>.
- Wang, P., Tang, C., Sun, K., Chen, Z., Xu, S., Shi, B., 2016. Advances on solidification/stabilization of sludge disposal. *J. Eng. Geol.* 24 (4), 649–660. <https://link.cnlki.net/doi/10.13544/j.cnki.jeg.2016.04.022>.
- Wang, Z., Xu, L., Liu, D., Zhang, Q., Hu, A., Wang, R., Chen, Y., 2021. Effects of air temperature and humidity on the kinetics of sludge drying at low temperatures. *Energies* 14 (22), 7722. <https://doi.org/10.3390/en14227722>.
- Waszczuk, L., Ogien, J., Pain, F., Dubois, A., 2023. Determination of scattering coefficient and scattering anisotropy factor of tissue-mimicking phantoms using line-field confocal optical coherence tomography (LC-OCT). *Journal of the European Optical Society-Rapid Publications* 19 (2), 39. <https://doi.org/10.1051/jeos/2023037>.
- Wen, H., Cheng, D., Chen, Y., Yue, W., Zhang, Z., 2024. Review on ultrasonic technology enhanced biological treatment of wastewater. *Sci. Total Environ.* 925, 171260. <https://doi.org/10.1016/j.scitotenv.2024.171260>.
- Weser, R., Woelkel, S., Wessely, B., Steinmann, U., Babick, F., Stintz, M., 2014. Ultrasonic backscattering method for in-situ characterisation of concentrated dispersions. *Powder Technol.* 268, 177–190. <https://doi.org/10.1016/j.powtec.2014.08.026>.

- Woo, D.K., Do, W., Hong, J., Choi, H., 2022. A novel and non-invasive approach to evaluating soil moisture without soil disturbances: contactless ultrasonic system. *Sensors* 22 (19), 7450. <https://doi.org/10.3390/s22197450>.
- Wotzka, D., Zmarzly, D., 2024. Low-cost device for measuring wastewater flow rate in open channels. *Sensors* 24 (20), 6607. <https://doi.org/10.3390/s24206607>.
- Xu, X., Cao, D., Wang, Z., Liu, J., Gao, J., Sanchuan, M., Wang, Z., 2019. Study on ultrasonic treatment for municipal sludge. *Ultrason. Sonochem.* 57, 29–37. <https://doi.org/10.1016/j.ulsonch.2019.05.008>.
- Yoo, J., Oshita, K., Takaoka, M., Kusakabe, T., 2022. Real-time measurement of the moisture contents of dewatered sewage sludge during thermal drying using a low-cost ECH2O EC-5 soil moisture sensor. *Dry. Technol.* 41 (8), 1321–1332. <https://doi.org/10.1080/07373937.2022.2148687>.
- Yuan, C., Zhang, J., Chen, L., Xu, J., Kong, Q., 2021. Timber moisture detection using wavelet packet decomposition and convolutional neural network. *Smart Mater. Struct.* 30 (3), 035022. <https://doi.org/10.1088/1361-655X/abdc08>.
- Yuan, H., Zhu, N., 2024. Progress of improving waste activated sludge dewaterability: influence factors, conditioning technologies and implications and perspectives. *Sci. Total Environ.* 912, 168605. <https://doi.org/10.1016/j.scitotenv.2023.168605>.
- Zhang, X., Dubois, F., Sauvat, N., Takarli, M., 2022. Hybrid numerical method for the ultrasonic wave propagation velocity in orthotropic materials. *Wood Sci. Technol.* 56 (6), 1605–1630. <https://doi.org/10.1007/s00226-022-01416-8>.
- Zhang, Y., Yao, Y., Yu, S., Huang, M., Lu, X., Lian, J., Xu, P., Rao, B., 2025. Rapid detection of sludge moisture content based on the frequency domain reflection. *Environ. Technol.* 1–14. <https://doi.org/10.1080/09593330.2024.2440657>.
- Zhi, Y., Xu, D., Jiang, G., Yang, W., Chen, Z., Duan, P., Zhang, J., 2024. A review of hydrothermal carbonization of municipal sludge: process conditions, physicochemical properties, methods coupling, energy balances and life cycle analyses. *Fuel Process. Technol.* 254, 107943. In: <https://doi.org/10.1016/j.fuproc.2023.107943>.
- Zhu, C., Zhang, P., Wang, H., Ye, J., 2018. Conditioning of sewage sludge via combined ultrasonication-flocculation-skeleton building to improve sludge dewaterability. *Ultrason. Sonochem.* 40, 353–360. <https://doi.org/10.1016/j.ulsonch.2017.07.028>.
- Zuljan, D., 2022. Effect of ultrasonic coupling media and surface roughness on contact transfer loss. *Cogent Engineering* 9 (1), 2009092. <https://doi.org/10.1080/23311916.2021.2009092>.